Biomed Microdevices (2006) 8: 167–176
DOI 10.1007/s10544-006-7712-8

Microfluidic handling of PCR solution and DNA amplification on a reaction chamber array biochip

Haiqing Gong · Naveen Ramalingam · Longqing Chen · Jing Che · Qinghui Wang · Yuming Wang · Xinhao Yang · Peng Huat Eric Yap · Chiew Hoon Neo

Abstract A microfluidic biochip for conducting an array of polymerase chain reaction (PCR) simultaneously was fabricated to understand the microfluidic loading process of PCR solution into microfabricated glass reaction chambers. The geometrical factors of the microfluidic structure, including the shape and depth of the microchamber, shape and size of the microchannels were investigated on the formation of air bubbles trapped within the microchamber during the PCR solution loading process. Furthermore, the effects of surface properties of the microfluidic structure, including hydrophilicity of the microchamber and inlet channel, and hydrophobicity of the outlet channel, on the loading of PCR solution, especially on the formation of air bubbles were studied. As a result, the surface wetting property of the microchamber was found to be the main reason for the formation of the air bubbles inside the microchamber during the loading of PCR solution in the biochips. A solution to avoid the air trapping has been proposed and investigated.

Keywords Microfluidics · Biochip · Air bubble trapping · Capillary flow · PCR (Polymerase Chain Reaction).

H. Gong (✉) · N. Ramalingam · L. Chen · J. Che · Q. Wang · Y. Wang · X. Yang · C. H. Neo
BioMEMS Laboratory, School of Mechanical and Aerospace Engineering, Nanyang Technological University, 50 Nanyang Avenue, Singapore 639798
e-mail: mhqgong@ntu.edu.sg

P. H. E. Yap
Defense Medical and Environmental Research Institute @ Defense Science Organisation, 27 Medical Drive, #13-00, Singapore 117510

1. Introduction

Biochip platform technology is widely used in micro-scale integrated biochemical analysis or synthesis systems, also referred as "lab-on-a-chip." A biochip normally consists of reaction chambers and fluid flow systems and the latter comprises of transport and separation channels for easy sample and reagent loading (Burns et al., 1996; Swerdlow et al., 1997; Unger et al., 2000; Lagally et al., 2000; Hong et al., 2003). In the area of molecular and cell biology, PCR (polymerase chain reaction) is a basic and key step in most of the protocols for molecular analyses that require an amplification of DNA or RNA. Standard PCR based DNA amplification involves liquid handling of reagent and DNA template solutions including measurement and mixing of PCR component solution volumes. The complete process relies on human intervention at several steps to transfer liquid, mix reagent and analyze results. The current trend of the PCR technology is to achieve miniaturization (Woolley et al., 1996; Belgrader et al., 1998; Northrup et al., 1998; Anderson et al., 2000) and high throughput gene amplification (Nagai et al., 2001; Matsubara et al., 2005). In comparison to conventional PCR, micro PCR allows much more precise temperature control and rapid DNA amplification (Taylor et al., 1997; Ibrahim et al., 1998; Northrup et al., 1998).

Immense efforts have been made to develop PCR-based biochips as a highthroughput platform, for analyses of thousands of genes in short time, and most of these devices required the use of a separated PCR sample loading into individual reaction wells in a PCR chip, similar to that used in a wellplate operation, or required costly liquid dispensing robot (Nagai et al., 2001; Matsubara et al., 2005). These high-throughput PCR-based system lacked a non-robotic based manual method to simultaneously load a nucleic-acid sample into a large number of reaction wells in micro and nanoliter

volume ranges and a manual method to simultaneously seal all these wells to avoid sample evaporation and PCR primer diffusion among interconnected microwells during PCR thermocycling. Microfluidics offers solution to the problems related to nucleic-acid sample loading (Lagally et al., 2000; Thorsen et al., 2002) and microreactor sealing for a large array of microreactors. We believe an air trapping phenomenon may be present in these microfluidic systems.

Successful amplification of DNA on high throughput PCR based biochips using microfluidics for sample and reagent loading depends on a complete loading of the PCR solution in microchambers without air trapping. If an air bubble is trapped inside a microchamber, the bubble may undergo expansion, contraction, and relocation inside the microfluidic network due to the large cyclic variation of temperatures within the PCR solution. The existence of these bubbles in the microchambers would be detrimental to the DNA amplification and subsequent DNA detection by real-time fluorescence monitoring. Hence, this phenomenon has to be avoided either through microfluidic geometric design or through surface property control of the microfluidics. It is critical that no air bubble is trapped inside the microchambers during the loading of PCR solution.

This paper presents some new developments of microfluidics PCR chips. The microfluidic chip presented combines a microfluidic channel network with an array of PCR microchambers. A microfluidic phenomenon on the PCR chip involving air bubble trapping in microchambers is described and discussed in this paper.

2. Materials and methods

2.1. Biochip design

The biochip layout having a variety of microchamber shapes was microfabricated using photolithography and glass etching processes, as shown in Fig. 1(a). An inlet channel is linked to all the microchambers through a set of corresponding inlet bridge channels for the distribution of the PCR solution into the microchambers by capillary force, as shown in Fig. 1(b). One or more outlet bridge channels linked the corresponding microchamber to the outlet channel for air venting during the PCR solution loading. As shown in Fig. 1(a), the microchamber of a variety of shapes were fabricated in the forms of square (530 μm in length and width), round circle (ö 510 μm), octagon (100 μm of each side), diamond (370 μm of each side), hexagon (290 μm of each side), vertically standing rectangle (350 μm $\times$ 50 μm), horizontally standing rectangle (920 μm $\times$ 510 μm) and semicircle with 3 outlet bridge channels (ϕ770 μm; each outlet bridge channel has 75 μm in width and 620 μm in length, and the distance between the bridge channel is 15 μm). The inlet and outlet channel shown in Fig. 1(b) has a width of 100 μm and a depth of 20 μm and the inlet and outlet bridge channels have a length of 30 μm, width of 550 μm and a depth of 20 μm. In Fig. 2(a), biochip layout i, ii, iii represent the variations in geometric characteristics of the inlet bridge channel, outlet bridge channel, and number of outlet bridge channels, respectively. In Fig. 2(b), the microchambers were etched to have a different depth from 20 μm to 200 μm to investigate the effect of the chamber depth on PCR solution loading.

2.2. Biochip fabrication

The distribution of the PCR solution into the microchambers was achieved by treating the surfaces of the inlet channels, inlet-bridge channels and microchambers with piranha solution (concentrated H_2SO_4 and H_2O_2 at a volumetric ratio of 70:30) and deionized water to make these surfaces hydrophilic. The PCR solution was confined within the microchambers by coating the surface of the air venting channel with a hydrophobic chemical. For simultaneous analysis of multiple gene targets, different primer sets were preloaded into different microchambers and dried. Following this, the etched glass chip was bonded at low temperature to a glass cover using a PCR chemistry compatible adhesive. The glass cover was fabricated with liquid injection and extraction ports.

2.2.1. Multilayer etching of glass for biochips

To fabricate the biochip, a glass slide (Corning 2947 MicroSlides 75 $\times$ 50 mm, 1 mm thick) was treated in acetone, and deionized water in an ultrasonic bath in a clean room environment (class 100) for half an hour. A metal mask was used to deposit a layer consisting of 300-Å Cr and 1000-Å Au under the Edwards Auto-306 e-beam evaporator (Edwards High Vac International, Crawley, UK). The glass slide patterned with Au/Cr was first spun with a layer ($1 \sim 2\mu$m) of positive photoresist (AZ7260, Synergy), prebaked at 100° C for 60 seconds, followed by UV exposure for about 5 seconds and then postbaked at 110°C for 60 seconds. Subsequently, the photoresist was developed in a photoresist developer (AZ300-MIF, Synergy) for about 1 minute. Finally, the patterned photoresist layer is hard-baked at 120°C for 5 minutes. The Au/Cr in the region of the channel was exposed, but the Au/Cr in the other region was covered by photoresist. The 6 exposed Au/Cr was then removed by chemical etching with gold etchant and chromium etchant, resulting in the exposure of the glass in the exposed region. Next, the exposed glass was etched in a slow stirring mixture of concentrated HF-HNO_3-H_2O (20:14:66, volume ratio). The channel depth during etching was monitored by a Dektak^3 surface profiler (Veeco, Plainview, USA) to establish the desired etch rate and etching period. The deeper chamber

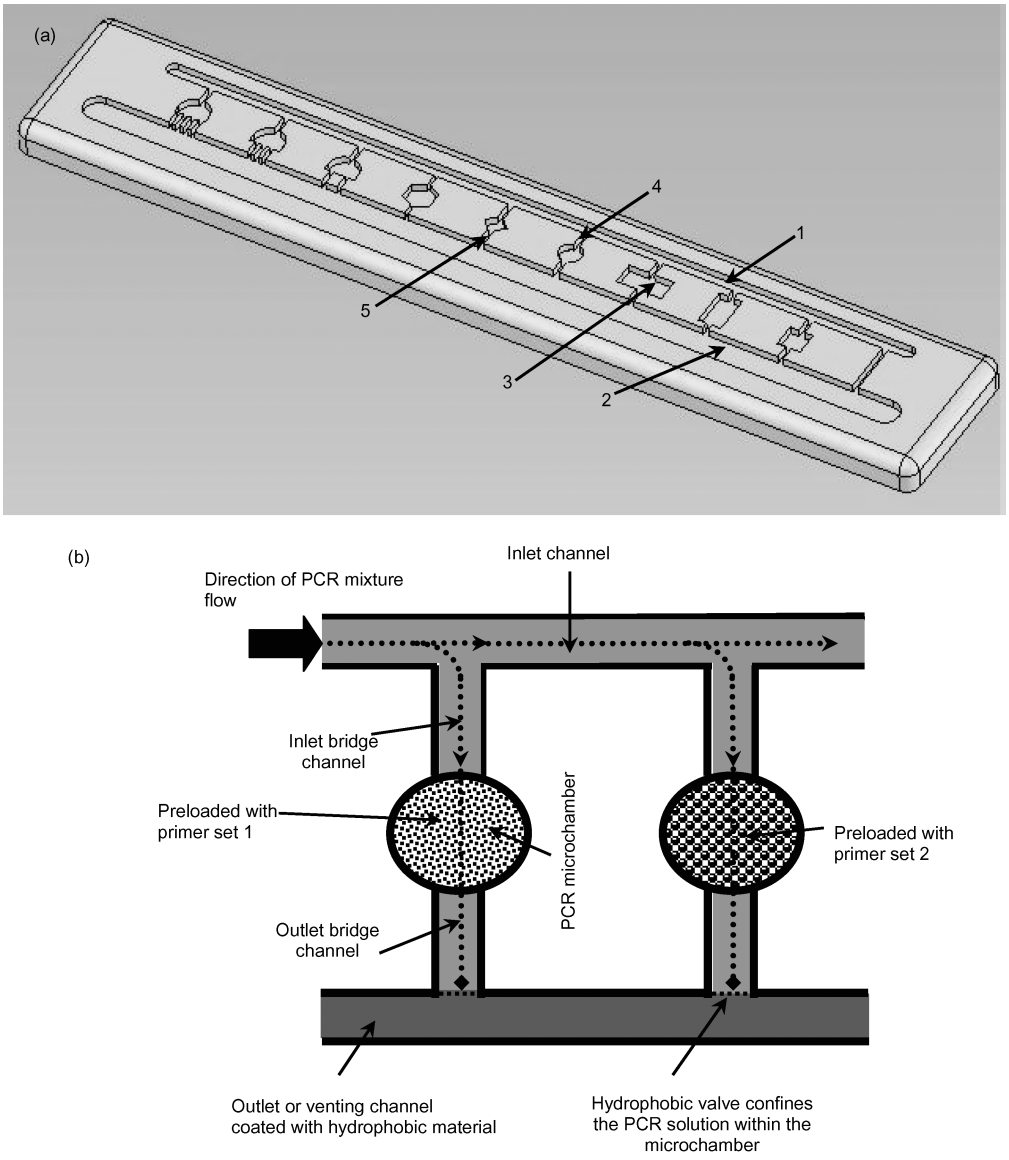

Fig. 1 Microfluidic biochip layout and the principle of PCR solution distribution: (**a**) An illustration of a microfluidic biochip showing inlet channel (1) for PCR solution loading, outlet channel (2) for air venting, PCR microchambers of various shapes (3), inlet bridge channel (4) connecting a microchamber with inlet channel and outlet bridge channel (5) connecting a microchamber with outlet channel. The biochip cover is not shown. (**b**) Distribution of PCR solution into microchambers for genetic testing of multiple DNA targets with different PCR primer sets (primer set 1 and 2)

shown in Fig. 2(b) was made using a multi-layer glass etching process. The fabrication process of the etched glass chip containing the microchannel and microreactor is shown in Fig. 3(a).

2.2.2. Selective biochip surface treatment for PCR solution containment

The flow of the PCR mixture on the hydrophilic chip surface can be achieved by capillary action, if the chip surface is thoroughly cleaned using the piranha solution and deionized water. However, containing the PCR mixture within the microchambers with a hydrophobic patch coated on the air venting channel surface is a challenging matter. We treated the air venting channel surface with EGC-1700 (kind gift from 3M Technologies Pte. Ltd., Singapore). Before the hydrophobic surface treatment, the glass slides were cleaned in the piranha solution and thoroughly rinsed with deionized water, and dried in an oven at 100°C at atmospheric pressure for 2 hrs. Following this, 1.5% of EGC-1700 in acetic acid was prepared and a thin layer of EGC-1700 was coated on the air venting channel surface. The schematic diagram of the hydrophobic coating on the air venting channel surface is shown in Fig. 3(b).

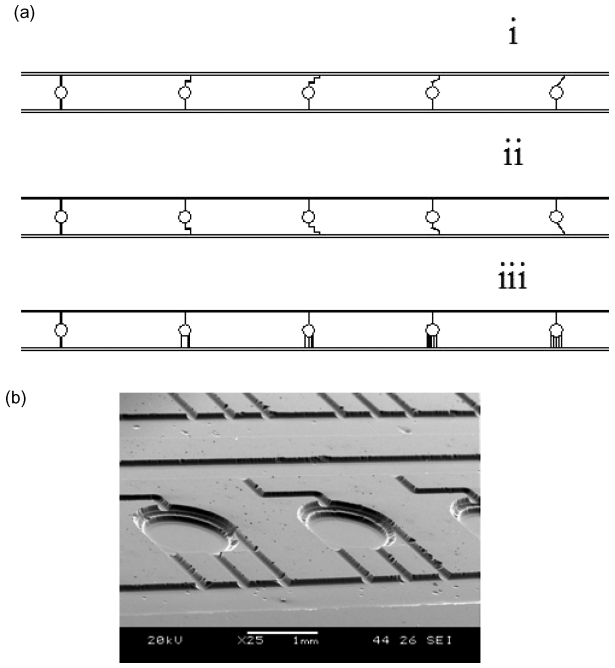

Fig. 2 A microfluidic biochip layout with variations for geometric features: (**a**) Variations in the inlet and outlet bridge channel geometries. i. Variations in inlet bridge channel; ii. Variations in outlet bridge channel; iii. Variations in number of outlet bridge channels. (**b**) Variation in microchamber depth, where the microchamber is deeper than channels using a multilayered glass etching process

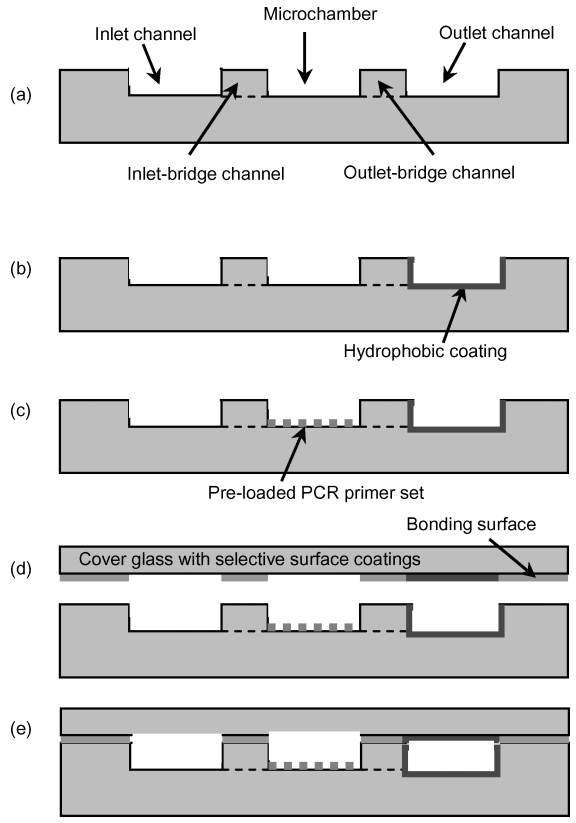

Fig. 3 Schematic diagram of microfabrication process for PCR microchip: (**a**) Layout of inlet, oulet, inlet-bridge, outlet-bridge and microchambers on an etched glass chip (**b**) EGC-1700 hydrophobic coating on the surface of the outlet channel. (**c**) PCR primer set deposition and drying on the surface of the microchamber. (**d**) Coating of EGC-1700 hydrophobic coating on cover slip region exposed to the outlet channel, and coating of PCR compatible adhesive in the bonding interface region (**e**) Bonding of etched glass chip with cover slip

2.2.3. PCR primer loading and biochip bonding

For simultaneous analysis of multiple gene targets on the same DNA template, different microchambers contained different PCR primer set. The PCR primer sets were loaded into the microchambers and then dried on the surface of the microchambers by incubating the chip at 40°C for 30 minutes [Fig. 3(c)]. Next, the microchip was either bonded with a glass slide or a plastic film using a hot melt adhesive compatible with PCR chemisty to form the closed chambers and channels [Fig. 3(d)]. The region of the glass slide exposed to the air venting channel was coated with the same hydrophobic chemical used to coat the surface of the air venting channel. A home-made heat laminating machine is set at 120°C to conduct the bonding of the cover layer which is with a PCR assay compatible hot-melt adhesive. The diffusion temperature of the adhesive is less than 90°C and the melting temperature is above 100°C. This is to ensure the integrity of the bonding during the PCR thermal cycling.

2.3. Operation of microchip

The PCR solution can be loaded along the inlet channel, through the inlet bridge channels to the microchambers. After filling the microchambers with the PCR solution, the both inlet and outlet channels were filled with mineral oil of PCR grade (Sigma, Singapore, M-8662) to isolate the microchambers. Following this, the injection and extraction port on the glass cover, exposed to the air was sealed using poly(dimethylsiloxane) (PDMS) to prevent oil leaking during PCR thermocycling, and the biochip containing PCR solution is now ready for thermocycling. Since the existence of the bubbles in the microchambers would be detrimental to the DNA amplification and subsequent DNA detection, the geometrical design of the microchip is one of the most important factors to avoid the trapping of air bubble. A direct flow visualization experiment using a video camera was conducted to investigate the effect of the geometrical factors on the air bubble trapping in a microchamber during the PCR solution loading into the 8 microchambers. The geometric factors include the shape of the microchamber, size and thickness of the microchamber, shape and size of the inlet channel(s), and shape and size of the outlet channel(s).

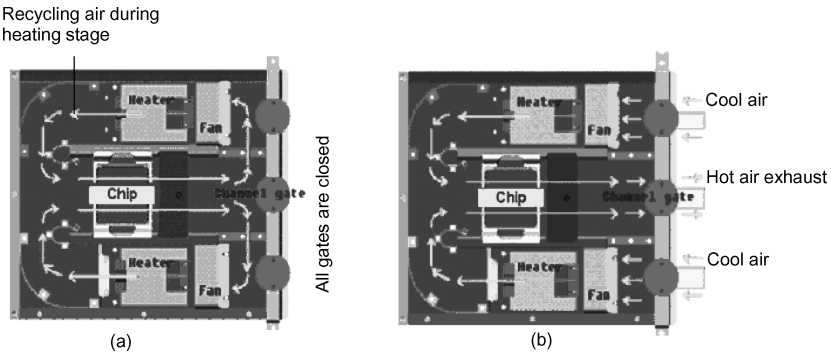

Fig. 4 Airflow paths for heating and cooling stages of thermocycling in PCR instrument (**a**) Top view of the thermocycling chamber showing airflow in convection channels during heating stage (The channel gates are closed) (**b**) Top view of the thermocycling chamber showing airflow in convection channels during cooling stage (The channel gates are open)

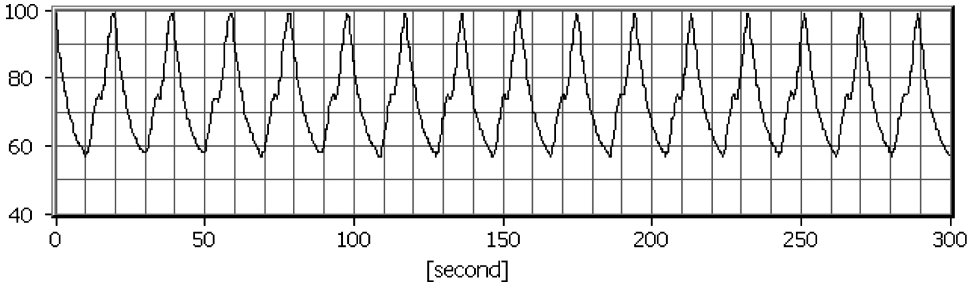

Fig. 5 Thermocycling temperature profile for PCR amplification on the fabricated biochip. The temperature holding time at each stage of 95°C (denaturation), 58°C (annealing) and 72°C (extension) was 2 seconds. A fast cycling condition of 8.6 cycles/min was achieved

2.4. PCR amplification instrument

A prototype PCR instrument using an air flow thermocycling for conducting PCR on the biochips was constructed and tested. The air inside the PCR thermocyling chamber containing the biochip was heated by a heating coil embedded in the thermocycling chamber and circulated by an embedded electric fan for air mixing. During the heating stage, a thermocycling chamber gate is closed and the heating coil heats the air inside the chamber, while during the cooling stage, the gate opens and the fan inside the chamber draws in the cool air to purge the hot air out of the chamber (Fig. 4). The entire PCR biochip was thermocycled with the same temperature profile. A thermocouple temperature sensor (Watlow Electric, Missouri, USA) was fixed in air near the surface of the PCR biochip to control the air temperature surrounding the PCR biochip. A PID temperature controller (Watlow Electric, Missouri, USA) was used to control air temperature.

2.5. PCR experiment

A 77 bp of the BNI-1 fragment of SARS DNA was PCR amplified in the PCR biochip. The sequences of forward and reverse primers were 5′-TTA TCA CCC GCG AAG AAG CT-3′ and 5′-CTC TAG TTG CAT GAC AGC CCT C-3′. The PCR mixture contained 10 mM Tris-HCl (pH 8.4), 50 mM KCl, 0.1% Triton X-100, 0.2 mM each of dATP, dCTP, dTTP and dGTP, 3 mM MgCl2, 0.3 μM each forward and reverse primer, 1 μg/μl of BSA, 0.1 U/μl of Taq DNA polymerase (Promega, Madison, USA), and 0.1 ng/μl of SARS DNA cloned in pGEM-3Z vector as template. For a clear flow visualization under a video camera, the PCR solution was added with a 0.2% blue dye.

To compare and validate the PCR on the microfabricated biochip, the BNI-1 fragment of SARS DNA was PCR amplified on a commercial instrument (Corbett Research, Sydney, Australia) with the following thermocycling profile: Initial denaturation at 95°C for 50 seconds followed by 40 cycles of denaturation at 95°C for 0 seconds, annealing at 58°C for 0 seconds and extension at 72°C for 2 seconds (for imaging of fluorescence emission on the chip). The same temperature profile was used for PCR amplification on the biochip (Fig. 5). The desired PCR product was confirmed by agarose gel electrophoresis.

3. Results and discussions

The first part of experiment was conducted to investigate the geometrical factors, including the shape, size and thickness of the microchamber, shape and size of the inlet channel(s), and shape and size of the outlet channel(s). By changing the depth (in the range of 20 $\sim$ 100 μm) and size of the chamber and inlet/outlet channel, the remaining variable is the flow speed of the PCR solution. As the depth of the microchamber and channel decreases, the loading speed in the microchips became higher. Similar results occured when the sizes of the chamber and channel were reduced. This is due to a higher capillary pressure in the chamber and channel when the chamber and channel decrease in size, resulting in easier loading of the PCR solution.

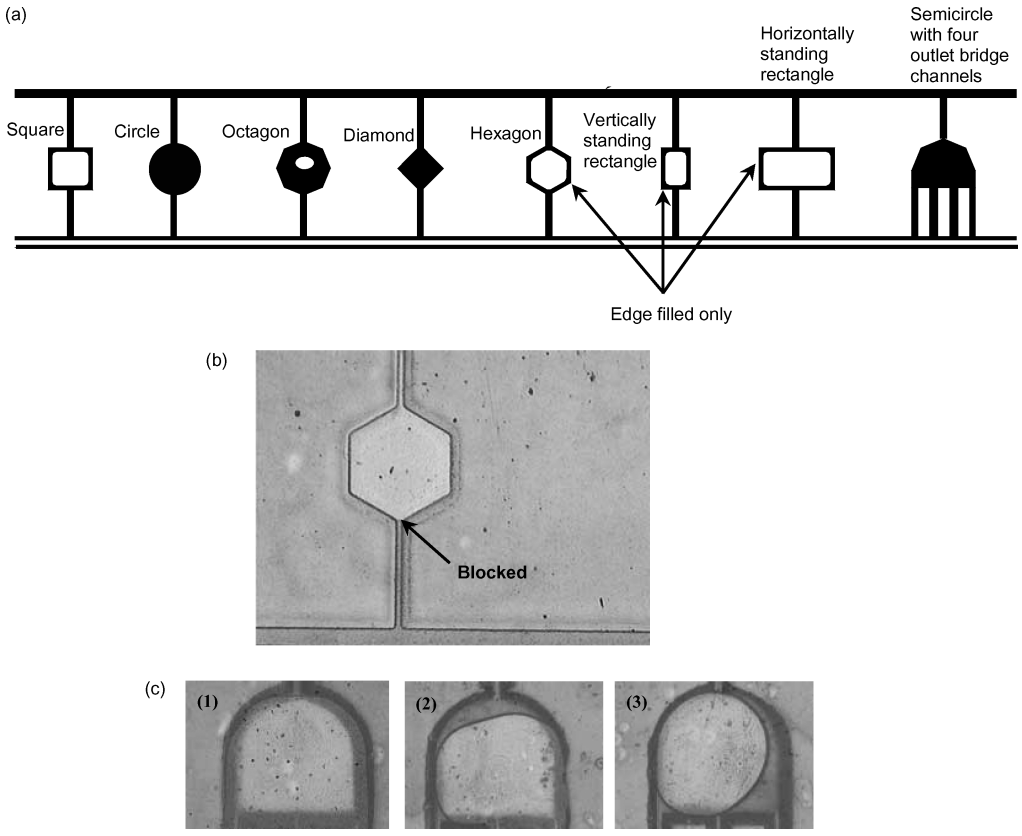

Fig. 6 A selected sample loading failure modes. (**a**) Effect of the shape of the microchamber on the loading of the PCR solution, where the black portion indicates the area filled with PCR solution. The sample loading failed for certain chamber geometries. The microchambers with shapes like square, hexagon, vertically standing rectangle, and horizontally standing rectangle were only filled in the area near the chamber sidewall. The off-sidewall area were not filled because of the air trapping caused by the blockage of the microchamber air venting exit by the fast moving liquid along the sidewall. (**b**) A sample loading failed when the sample stopped at the exit of the inlet bridge channel and failed to flow into the microchamber. This failure is contributed by both narrow inlet channel and lack of high hydrophilicity of the glass surface of the microchamber. (**c**) Video snapshots of a liquid loading sequence in a semicircle microchamber entrapping air in the central portion of the microchamber due to non-uniform hydrophilicity on the surface of the microchamber

During the loading process for chamber geometries shown in Fig. 6(a), it was observed that the loading speed was very different for microchambers of different shapes. The loading speed for different shapes of microchambers is summarized in Table 1. We found that only certain microchambers, including the semi-circle, circle, diamond and octagon shape, could be loaded with the PCR solution, in a time of 0.9, 1.8, 3.7 and 5.0 seconds, respectively. The other types of microchambers listed in Table 1, were filled with PCR solution only in the edge area along the sidewall of the microchambers. We also found that changing the shapes and numbers of the inlet and outlet bridge channels had no obvious influences on the loading speed. However, the shapes and depth of the chamber, especially the deep microchamber chip (as shown in Fig. 2(b)), shape and size of the inlet channel(s), and shape and size of the outlet channel(s), and the surface wetting properties of the microchambers greatly affected the PCR solution loading and the formation of air bubbles. For example, we noticed that the microchambers with shapes like square, hexagon, vertically standing rectangle, and horizontally standing rectangle were not even filled, since the PCR solution simply stopped at the exit of the inlet bridge channel before entering the chamber, as shown in Fig. 6(b).

Table 1 The loading speed of PCR solution at the microchambers with different shapes

Chamber geometry	Loading speed (mm/sec)
Semi-circle	0.9
Circle	1.8
Diamond	3.7
Octagon	5.0
Square	Edge filled only
Hexagon	Edge filled only
Vertically standing rectangle	Edge filled only
Horizontally standing rectangle	Edge filled only

For the air trapping inside the microchambers, it was found that the deeper the microchamber, the more difficult for the PCR solution to flow into the chamber without air bubble trapping. A typical air trapping scenario is shown in

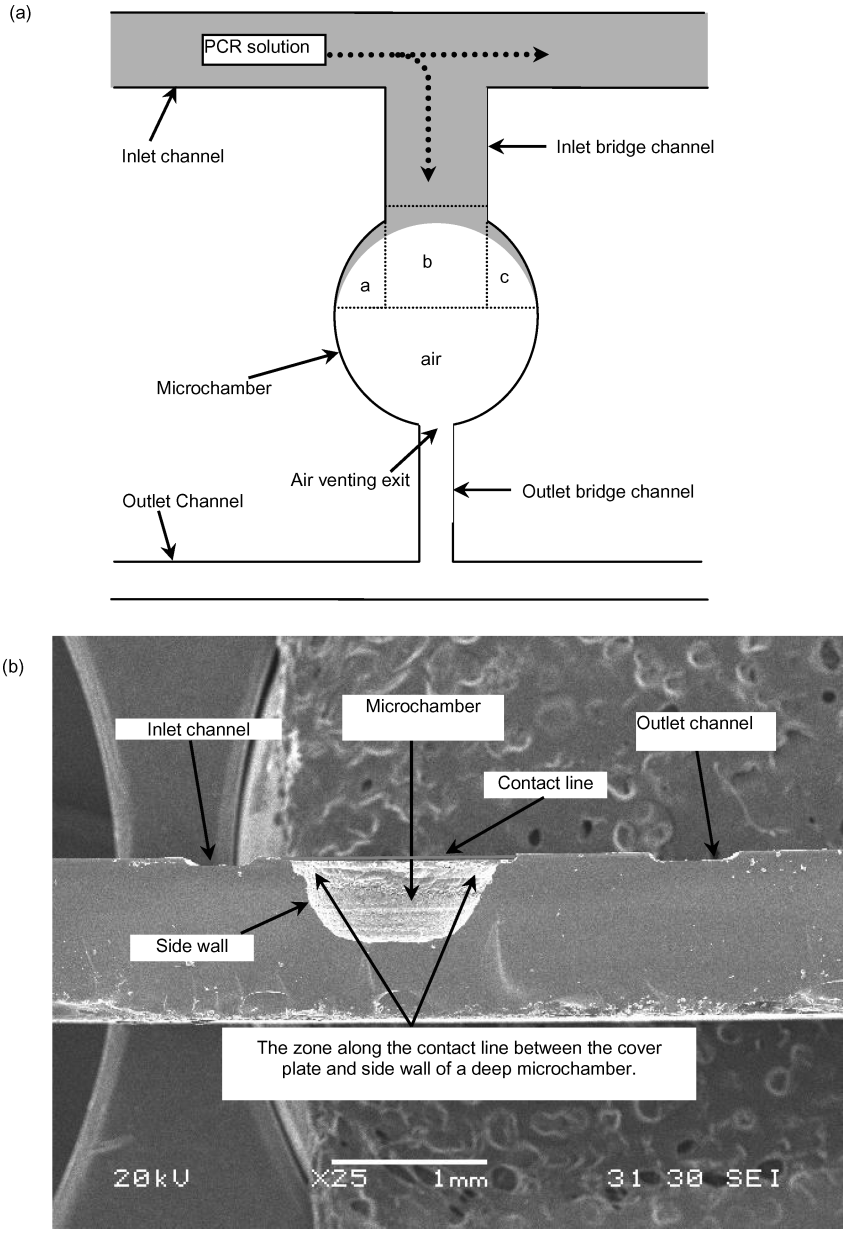

Fig. 7 A faster movement of liquid along the edge of a microchamber which may block the air venting exit and cause the air trapping in the central part of a microchamber. (a) A faster movement of liquid was observed in the zone along the side wall of a shallow microchamber. (b) A cross-sectional image of a glass chip showing the deep etched microchamber and the inlet and outlet channels. A faster movement of liquid was observed in the zone along the contact line between the cover plate and side wall of a deep microchamber

Fig. 6(c). During the PCR solution loading process for all types of microchambers, an interesting phenomenon was found that, after entering the microchamber of a shallow depth similar to that of the inlet channel, the PCR solution tended to flow along the side wall region of the microchamber (Zone a and c in Fig. 7(a)) at a much higher speed than flowing in the central region of the chamber (Zone b in Fig. 7(a)). For a microchamber of a much larger depth than that of the inlet channel, we observed that a faster liquid movement occurred in the zone along the contact line between the cover plate and the side wall of the deep microchamber, as shown in Fig. 7(b), and subsequently block the air venting exit before the air in the microchamber is fully vented. The detailed video image sequence of the air trapping processes is shown in Fig. 8(a). The liquid reaches the outlet venting channel from the chamber side wall earlier than the central region of the chamber, resulting in an amount of air trapped inside the chamber. However, it was found that this air-trapping phenomenon is generally independent of the chamber shape. We speculate that when PCR solution flows into the microchamber region, the PCR solution has a lower effective contact angle on the edges of the well as compared to the area off the edges due to the existence of the side wall in addition to the upper and bottom microchamber surface. Negative effect of the air bubble trapping inside the microchamber is shown in Fig. 9, where the fluorescence image of the chip shows the lost of PCR solution in some microchambers due to expansion of trapped air bubble during PCR thermal

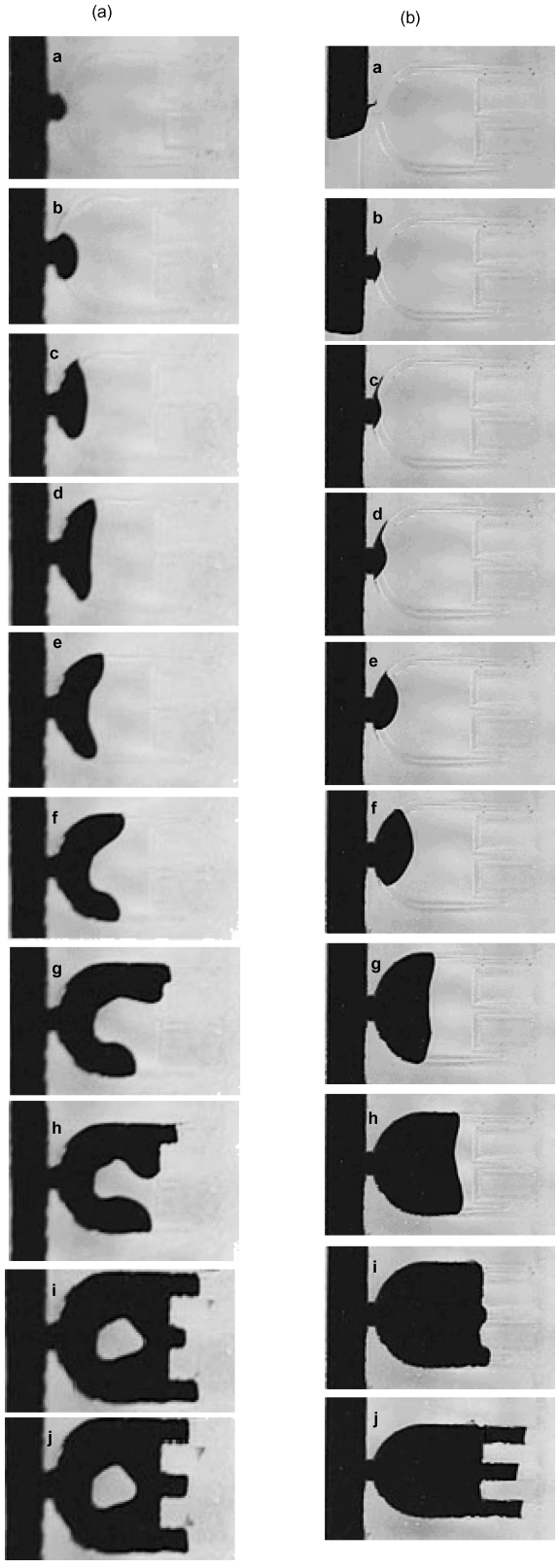

Fig. 8 Video snapshots of the sequence of the PCR solution loading in a microchamber showing the faster movement of liquid along the edge of the microchamber entrapping air in the central portion of the microchamber. (**a**) Formation of trapped air bubbles (**b**) No air trapping due to a highly hydrophilic surface of the microchambers and cover slip

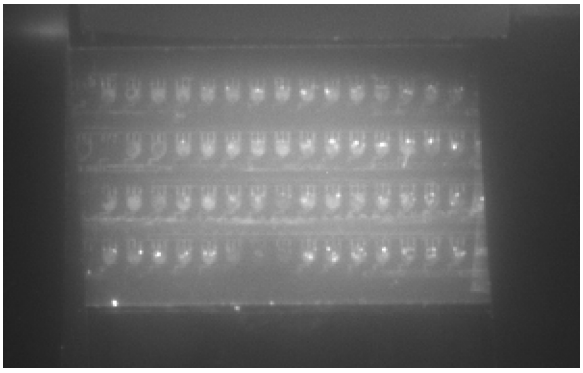

Fig. 9 The fluorescence image of the chip shows the lost of PCR samples in some microchambers due to expansion of trapped air bubble during PCR thermal cycling

cycling when the PCR solution temperature is raised above 90°C.

Some factors affecting the PCR solution loading are the microchamber surface roughness and surface treatment. When the microchamber surface was treated to be highly hydrophilic, the PCR solution could flow into the chamber smoothly and rapidly without trapping of air bubble. The detailed sample loading process is shown in Fig. 8(b), where a semi-circle chamber was fully loaded with the PCR solution. Additional experiments were conducted to investigate the surface properties of the biochip, which includes the hydrophilicity of the microchamber, inlet channels, the inlet-bridge channels, and the chip cover surface exposed to the microchamber, and the hydrophobicity of the outlet channels as well. We found that the air trapping was less dependent of the hydrophilicity of the microchamber surface than the difference in hydrophilicity between the microchamber surface and chip cover surface (exposed to the microchamber). It was observed that, given a hydrophilicity of the microchamber surface, a more hydrophilic chip cover surface would result in less likelihood of trapping the air bubbles. We also observed that a low level of roughness of the chamber surface played little role on influencing the surface free energy.

Another observation was that, even on a hydrophilic treated glass microchamber surface, it was difficult to achieve a uniform hydrophilicity and a corresponding uniform flow speed across the microchamber during the PCR solution loading process. Figure 10 shows a successful PCR solution loading process in the semicircle chamber, where the flow front movement is neither constant with time nor uniform across the microchamber. Figure 11 shows the fluorescence image of the chip with an improved sample loading into microchambers, where there was no significant purging of the PCR solution from microchambers by air bubble expansion during the PCR thermal cycling. To validate the PCR amplification on the fabricated biochip, the PCR product was manually

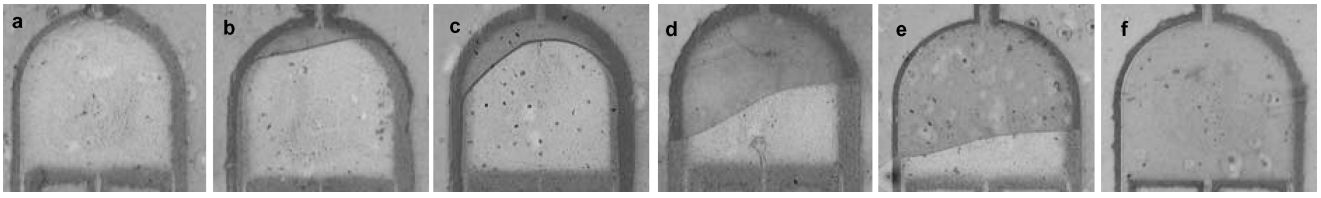

Fig. 10 The loading process of PCR solution in a semicircle chamber, in which it is difficult to generate a hydrophilic coating to enable a constant and uniform movement speed for the loading of the PCR solution

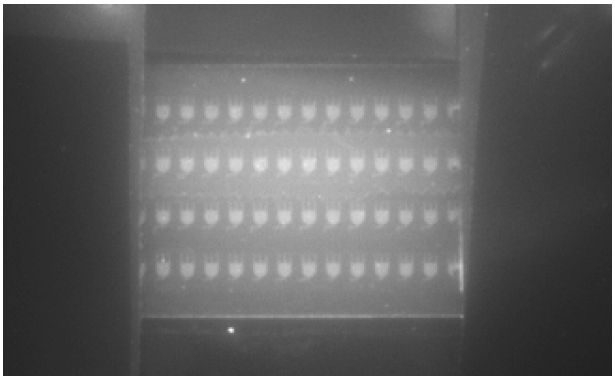

Fig. 11 A fluorescence image of the chip showing the minimum air trapping during PCR solution loading into microchambers, and an improved fluorescence emission during PCR thermal cycling

collected, pooled and analyzed on a 3% agarose gel electrophoresis (Fig. 12).

4. Conclusion

By varying the geometrical parameters and the surface wetting properties of the glass etched microfluidic structure, certain insights were obtained about air trapping in microchambers during the loading process of the PCR solution in a microPCR chip. The size of the microchamber, shape and size of the inlet, outlet and bridge channels were found to be little or no influence on the formation of trapped air bubbles in the microchamber. However, they had influence on the speed of PCR solution loading. We also found that the thickness of the microchamber has some effect on the loading of the PCR solution and the air trapping in the microchamber. In general, the deeper the microchamber, the more difficult for the PCR solution to flow into the chamber and avoid the air trapping. Furthermore, the surface wetting properties of the microchambers and the cover layer were found to have a major influence in the formation of trapped air bubbles during the loading of the PCR solution. When the microchambers as well as the inlet bridge channels were treated to be highly hydrophilic, the air bubbles trapping could be avoided or minimized during the loading of the PCR solution.

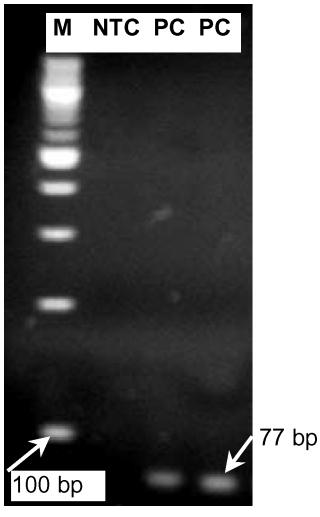

Fig. 12 The PCR product on the fabricated biochip was pooled together and analyzed by 3% agarose gel electrophoresis. NTC is the non-template control. PC is the positive PCR control. M is the 100 bp molecular marker

Acknowledgment The authors acknowledge the financial support of the Agency for Science, Technology and Research, Singapore (Project NSTB/43/11/4-1).

References

R.C. Anderson, X. Su, G.J. Bogdan, and J. Fenton, Nucleic Acids Res **28**, E60 (2000).

P. Belgrader, W. Benett, D. Hadley, G. Long, R. Mariella, Jr., F. Milanovich, S. Nasarabadi, W. Nelson, J. Richards, and P. Stratton, Clin Chem **44**, 2191 (1998).

M.A. Burns, C.H. Mastrangelo, T.S. Sammarco, F.P. Man, J.R. Webster, B.N. Johnsons, B. Foerster, D. Jones, Y. Fields, A.R. Kaiser, and D.T. Burke, Proc Natl Acad Sci U S A **93**, 5556 (1996).

J.W. Hong, and S.R. Quake, Nature Biotechnology **21**, 1179 (2003).

M.S. Ibrahim, R.S. Lofts, P.B. Jahrling, E.A. Henchal, V.W. Weedn, M.A. Northrup, and P. Belgrader, Anal Chem **70**, 2013 (1998).

E. Lagally, Peter C. Simpson, Richard A. Mathies, Sensors and Actuators B **63**, 138 (2000).

Y.K.K. Matsubara, Masaaki Kobayashi, Shouhei Yamanura, Yasutaka Morita, Eiichi Tamiya, Biosensors and Bioelectronics **20**, 1482–1490 (2005).

H. Nagai, Y. Murakami, Y. Morita, K. Yokoyama, and E. Tamiya, Anal Chem **73**, 1043 (2001).

M.A. Northrup, B. Benett, D. Hadley, P. Landre, S. Lehew, J. Richards, and P. Stratton, Anal Chem **70**, 918 (1998).

H. Swerdlow, B.J. Jones, and C.T. Wittwer, Anal Chem **69**, 848 (1997).
T.B. Taylor, E.S. Winn-Deen, E. Picozza, T.M. Woudenberg, and M. Albin, Nucleic Acids Res **25**, 3164 (1997).
T. Thorsen, S.J. Maerkl, and S.R. Quake, Science **298**, 580 (2002).
M.A. Unger, H.P. Chou, T. Thorsen, A. Scherer, and S.R. Quake, Science **288**, 113 (2000).
A.T. Woolley, D. Hadley, P. Landre, A.J. deMello, R.A. Mathies, and M.A. Northrup, Anal Chem **68**, 4081 (1996).